Bio-inspired design of NiFeP nanoparticles embedded in (N, P) co-doped carbon for boosting overall water splitting

Xiangrui Zhang, Xue-Rong Shi[*], *Peijie Wang, Zhiyu Bao, Mengru Huang, Yanan Xu, Shusheng Xu*[*]
School of Materials Science and Engineering, Shanghai University of Engineering Science, Shanghai 201620, China
*Corresponding authors.
Email: shixuer05@mails.ucas.ac.cn; xushusheng@sues.edu.cn

Content

Chemical and Material

$Ni(NO_3)_2$ $6H_2O$ (99%) and $FeCl_3$ $6H_2O$ (99%) were purchased from Shanghai Aladdin Biochemical Technology Co., Ltd. Carbon nanotubes (CNT), chitosan (CTS) and phytic acid (PA) (70%) were purchased from from Shanghai Titan. The other chemicals were analytical grade and used without further purification.

Electrochemical measurements

Firstly, the glassy carbon electrode (GCE, 5 mm in diameter) was polished with 0.05 μm alumina slurry until a mirror-shaped surface was acquired. Then the electrode was washed alternately with ethanol and ultra-pure water, and finally dried at room temperature. The as-prepared sample (2 mg) and 1 mg Secco piano black was ultrasonically dispersed in the mixed solution of ethanol (390 μL) and Nafion (5 wt%, 10 μL) to obtain a homogeneous ink. Then, the GCE was modified with 10 μL ink and dried at room temperature before measurements.

Electrochemical performance of all electrodes was determined on an electrochemical working station (Chenhua CHI660E, Shanghai, China) by a three-electrode system. A carbon rod is used as the counter electrode. Hg/HgO (1 M KOH) is employed as the reference electrode. The modified GCE with catalysts (loading: 0.26 mg cm^{-2}) was used as the working electrode. The electrolytes are 1 M KOH, and 1 M KOH + 0.5 M (NaCl). The LSV curves were measured with a scanning rate of 5 mV/s. Electrochemical impedance spectroscopy (EIS) measurements were performed at frequency from 100000 to 0.1 Hz. Electrochemical experiments were carried out with iR compensation (95%). The Tafel slope b was estimated using $\eta = a + b \log|j|$. The potentials in this work were adjusted with reversible hydrogen electrode (RHE):

$$E(RHE) = E(Hg/HgO) + 0.098 + 0.059 \times pH$$

To prepare Pt/C or RuO_2 electrode, 2 mg catalyst samples (Pt/C or RuO_2 powder) and 1 mg Secco piano black were added into 390 μL ethanol solution, ultrasonically dispersed for 30 min, then mixed with 10 μL Nafion, and ultrasonically dispersed for another 20 min to form the ink. The 10 μL of the mixed ink was dropped onto GCE and dried in air.

Characterization

The morphology of the materials is investigated using a scanning electron microscope (SEM, Ultra-55, Carl Zeiss, Germany) with a 3 kV accelerating voltage and secondary electron measurement mode. The morphology and element distribution in $Ni_{0.8}Fe_{0.2}P$-C were further explored using a transmission electron microscope (TEM, FEI Talos F200X G2, America) with a 200 kV accelerating voltage where the elemental distribution was recorded by a dark field mode. Powder X-ray diffraction (XRD, Rigaku Ultima IV diffractometer, Japan) patterns were analyzed to determine the crystal structure and phase composition of the materials using a Cu Kα (λ = 0.154 nm) radiation source generated at 30 kV and 25 mA, listed as Bragg measurement, in a 2θ scanning range of 10-90 °at a scanning speed of 5 °min^{-1}. The detector is a Detex Ultra one-dimensional semiconductor high-speed array detector. The Jade software is used to analyze data. X-ray photoelectron spectroscopy (XPS, Thermo Scientific K-Alpha+, Thermo) in the chamber is recorded with a non-monochromatic Al Kα X-ray source ($h\upsilon$ = 1486.6 eV) at 12 kV and filament current of 6 mA. The analyzer is operated at a constant pass energy of 50 eV. The binding energy is corrected based on the binding energy of C1s (284.8 eV). Relevant porosity data were obtained using the nitrogen adsorption/desorption isotherm measurement on a JW-BK122W equipment at 77 K. Inductively coupled plasma mass spectrometry (ICP-MS, Agilent-7700) was used to determine the Fe/Ni ratio of $Ni_{0.8}Fe_{0.2}P$-C.

Calculation details

The cutoff energy for the plane wave basis set was fixed at 400 eV. Force converged criterion for geometry optimization is 0.03 eV/Å. A Monkhorst-Pack grid of 3 × 3 × 1 and 1 × 1 × 1 were employed for the structural optimization of the FeP(121) and (carbon sheet-) TMPs composite model, respectively. For electronic properties calculations of FeP(121)-Ni_2P(111)/NPC, a 4 × 2 × 1 k-point sampling was used. Vacuum layers of 20 Å were used. The topest half of the total metal-P layers and adsorbates are allowed to relax during the geometry optimization. For the composite model, only the 12 atoms in the bottom layer is fixed to keep the shape without collapse and all the other atoms are allowed to relax during the optimization. For the

N-graphene, 3N model including two pyridine N, one pyrrole N, and one C defect model is built due to the vital role of the pyrrole N and C defects.

Figure S1. Synthesis of the NiFeP-C nanoparticles.

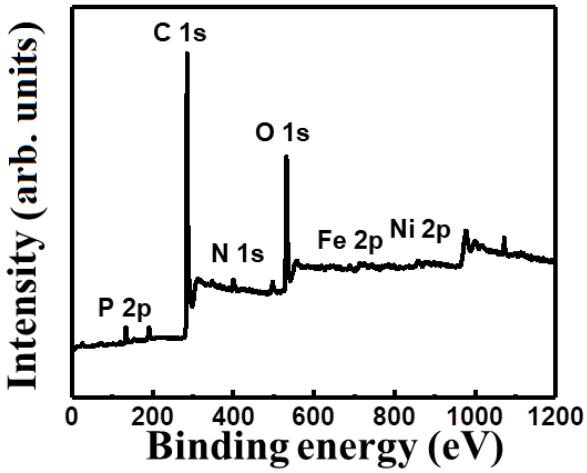

Figure S2. XPS survey of $Ni_{0.8}Fe_{0.2}P$-C.

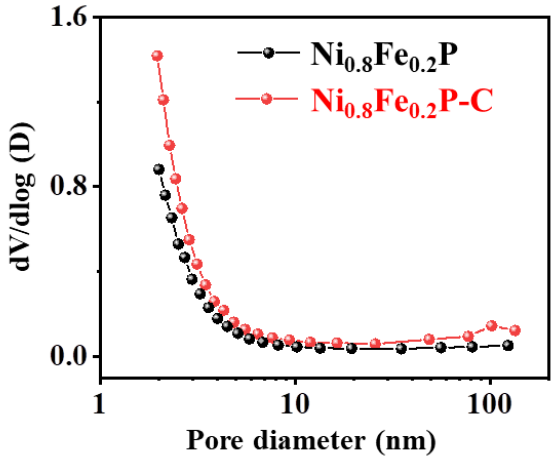

Figure S3. Pore size distribution profiles of $Ni_{0.8}Fe_{0.2}P$ and $Ni_{0.8}Fe_{0.2}P$-C.

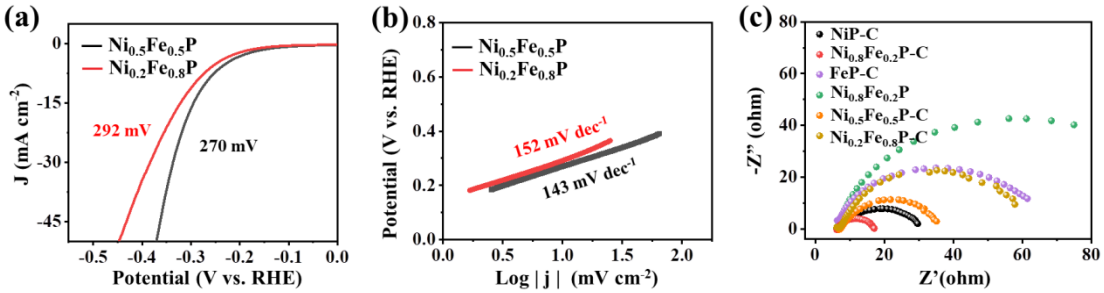

Figure S4. (a) Polarization curves of HER with marked η_{10} values and (b) Tafel slopes of $NiFe_{0.5}P$-C and $Ni_{0.2}Fe_{0.8}P$-C; and (c) Nyquist plots in 1.0 M KOH.

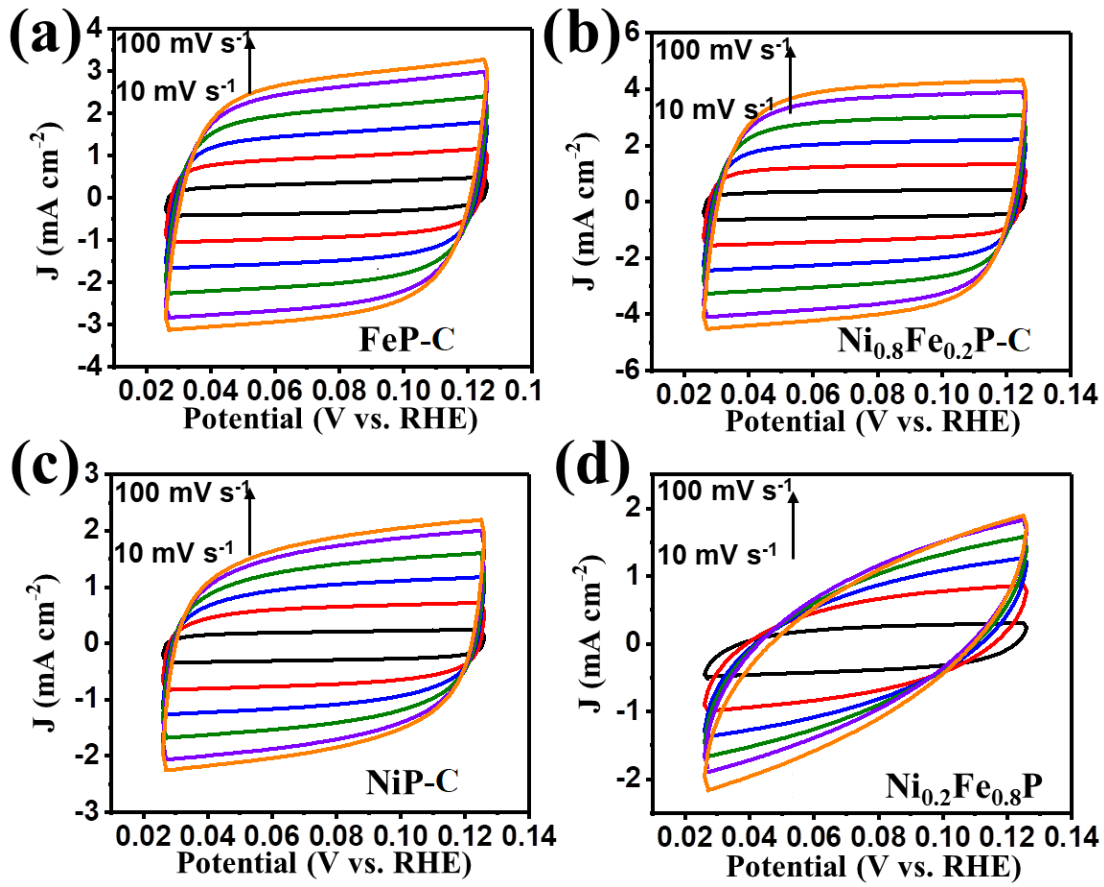

Figure S5. Cyclic voltammograms (CV) curves in 1.0 M KOH for (a) NiP-C; (b) $Ni_{0.8}Fe_{0.2}P$-C; (c) FeP-C; (d) $Ni_{0.8}Fe_{0.2}P$ at various scan rates (10, 30, 50, 70, 90, and 100 mV s^{-1}) under OER working condition in an alkaline solution.

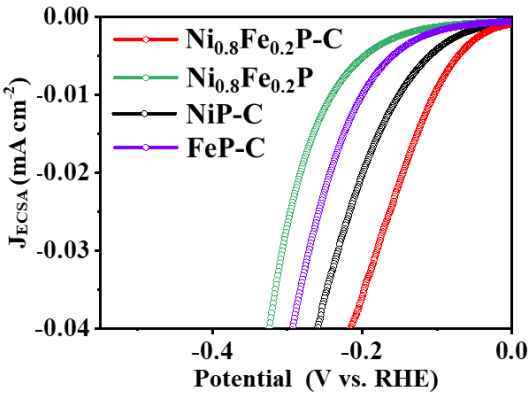

Figure S6. ECSA-normalized LSV curves of HER in 1.0 M KOH.

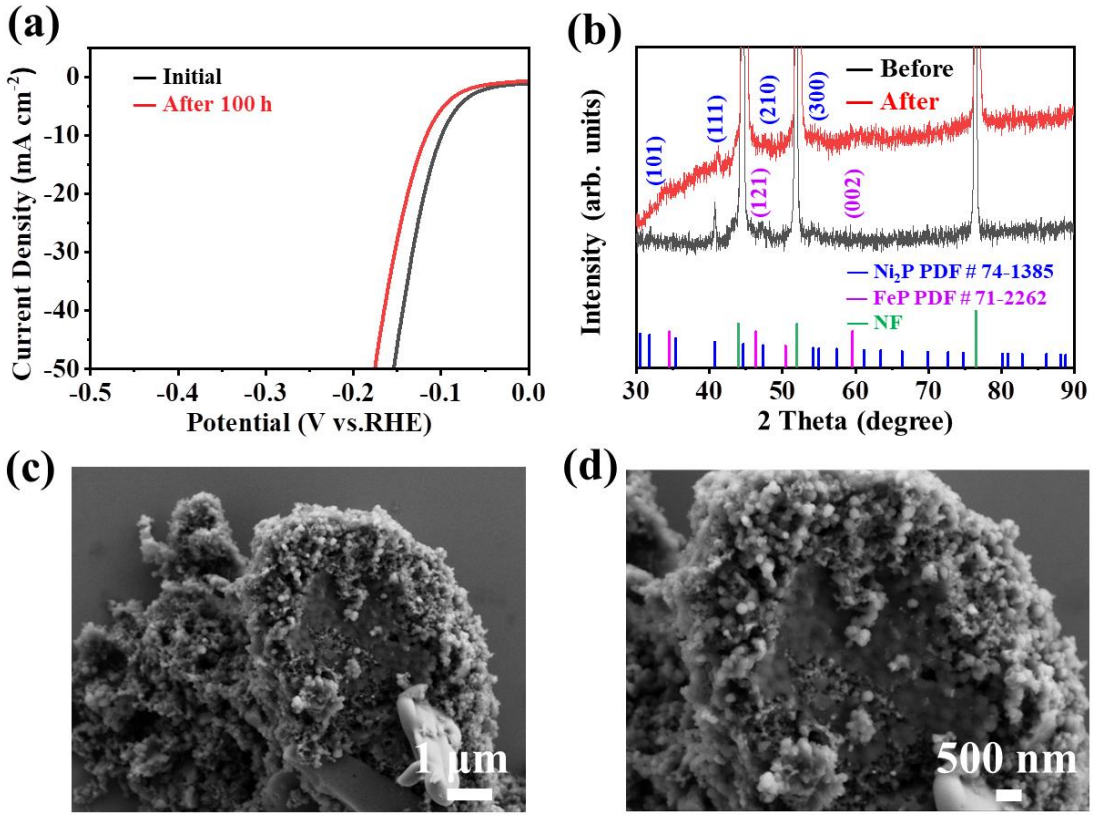

Figure S7. (a) The polarization curves and (b) XRD patterns of the $Ni_{0.8}Fe_{0.2}P$-C before and after 100 h long-term stability (alkaline). (c, d) SEM images after the HER stability test in 1.0 M KOH solution.

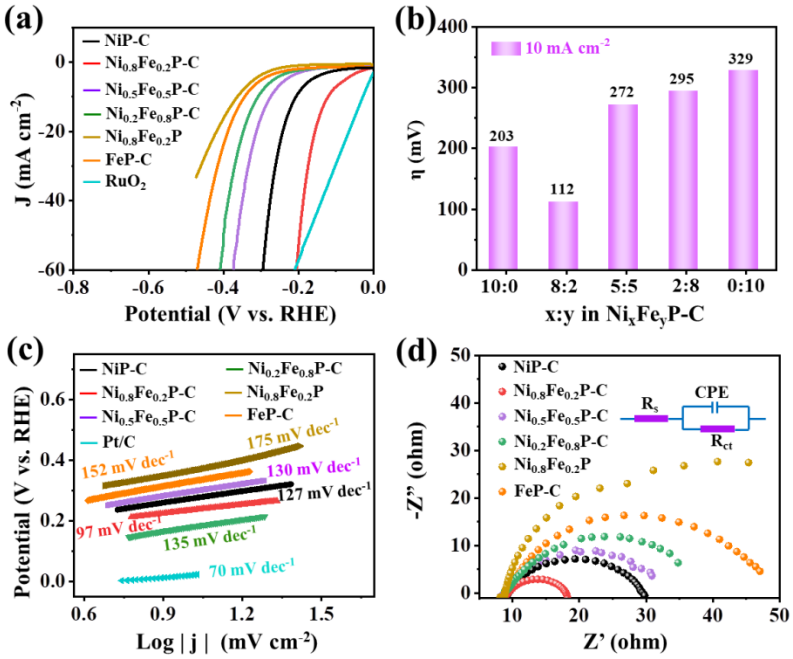

Figure S8. (**a**) Polarization curves of in alkaline simulated seawater; (**b**) Required overpotential (η) at current densities of 10 mA cm^{-2}; (**c**) Corresponding Tafel plots; (**d**) Nyquist plots (inset: the equivalent circuit diagram) for HER.

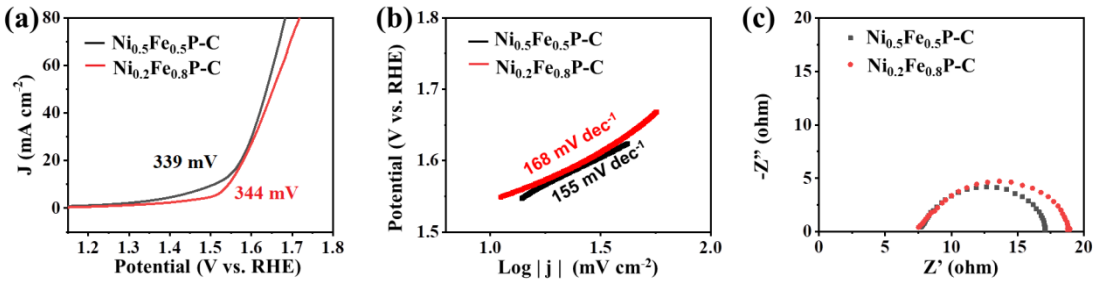

Figure S9. Polarization curves of OER in 1.0 M KOH of $Ni_{0.5}Fe_{0.5}P$-C and $Ni_{0.2}Fe_{0.8}P$-C.

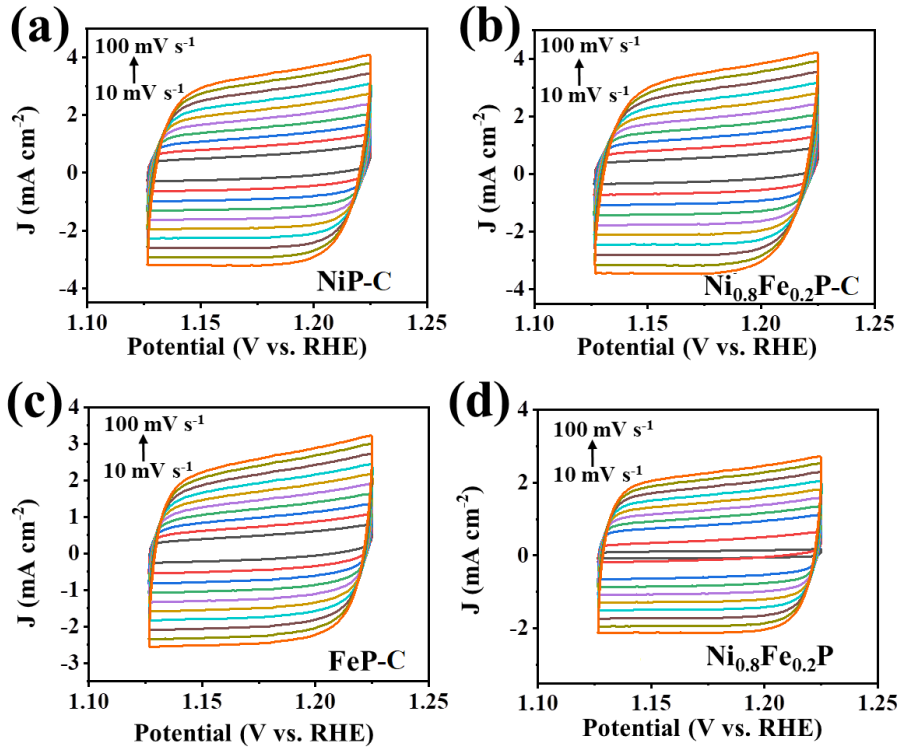

Figure S10. Cyclic voltammograms (CV) curves of (a) NiP-C; (b) $Ni_{0.8}Fe_{0.2}P$-C; (c) FeP-C; (d) $Ni_{0.8}Fe_{0.2}P$ at various scan rates (10-100 mV s^{-1}) under OER working condition in an alkaline solution.

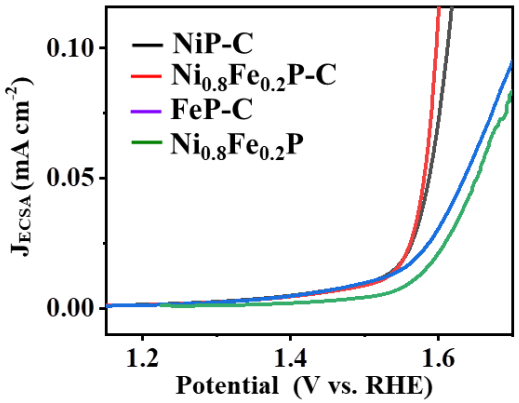

Figure S11. ECSA normalized LSV curves of OER in 1.0 M KOH.

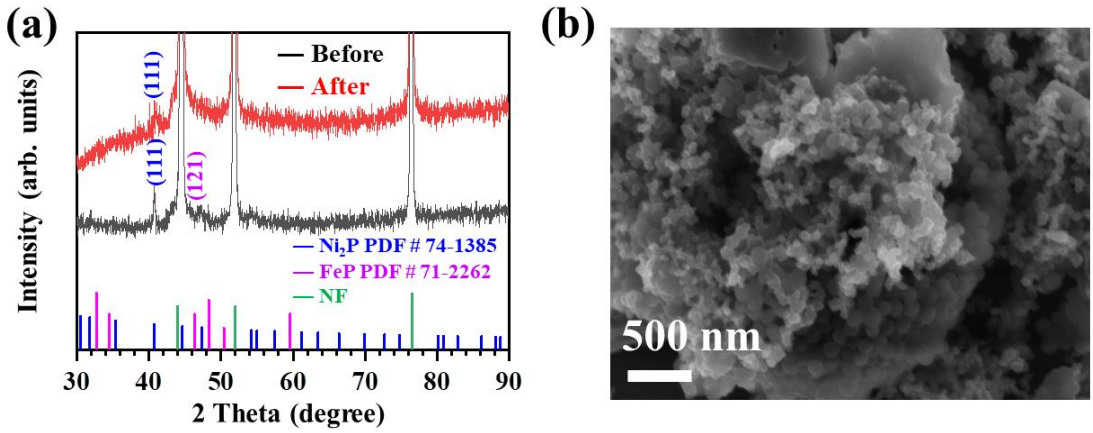

Figure S12. (a) XRD patterns of the $Ni_{0.8}Fe_{0.2}P$-C/NF before and after OER stability test (alkaline). (b) SEM images after the OER stability test in 1.0 M KOH solution.

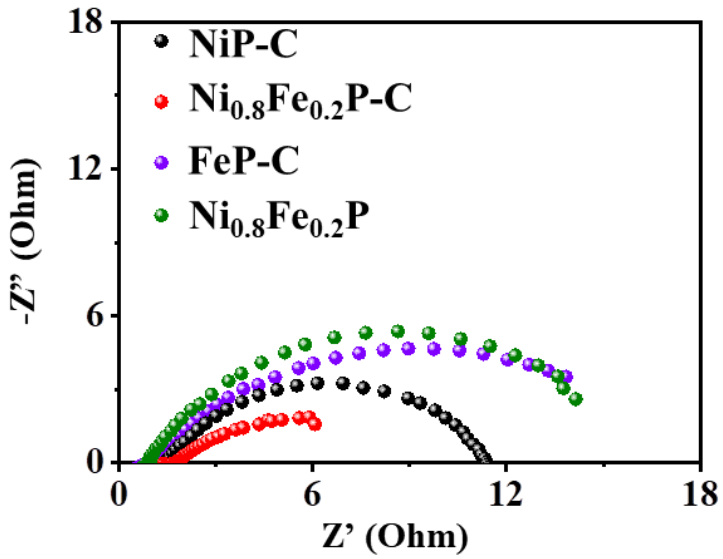

Figure S13. Nyquist plots for OER in 1.0 M KOH.

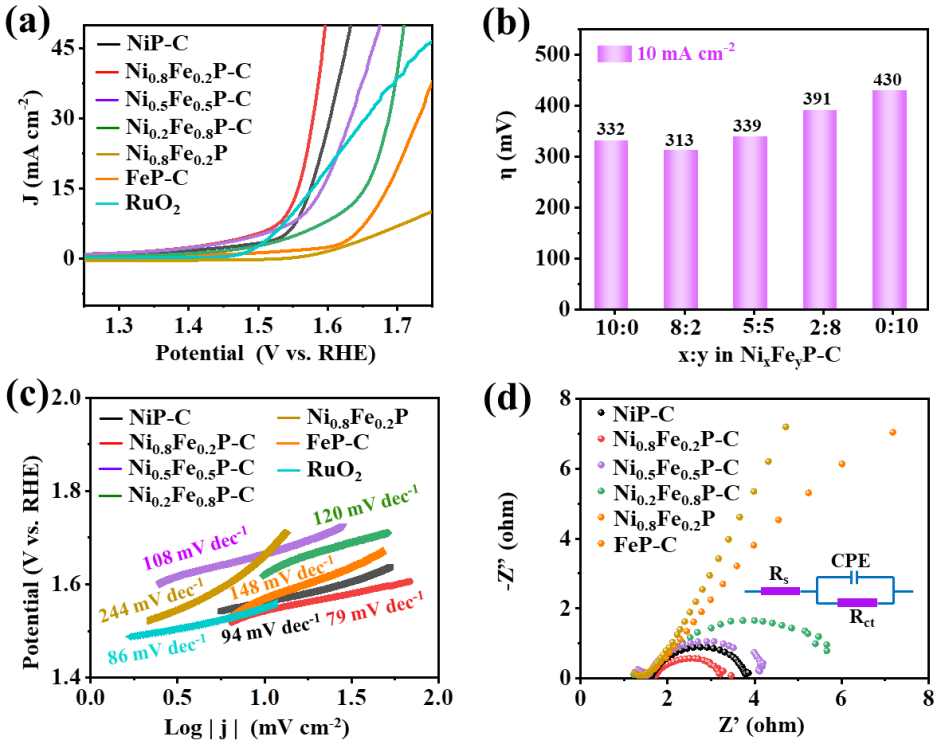

Figure S14. (**a**) Polarization curves of in alkaline simulated seawater; (**b**) Required overpotential (η) at current densities of 10 mA cm^{-2}; (**c**) Corresponding Tafel plots; (**d**) Nyquist plots (inset: the equivalent circuit diagram) for OER.

Figure S15. The photograph of overall water splitting powered by a battery with a nominal voltage of 1.5 V.

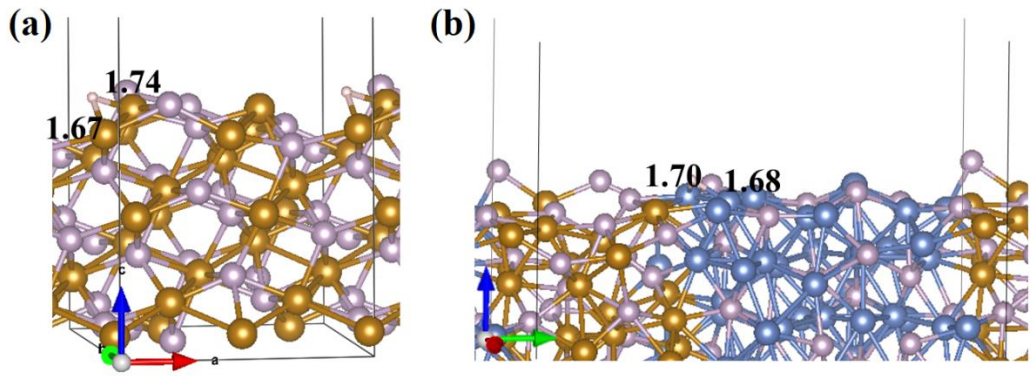

Figure S16. (**a**) H adsorption on the bridge site of Fe-Fe on FeP(121); (**b**) H adsorption on the hollow site of NiNiFe on Ni_2P(111)-FeP(121).

Table S1. Element contents of $Ni_{0.8}Fe_{0.2}P$-C based on XPS.

Sample	Ni (at%)	Fe (at%)	P (at%)	C (at%)	O (at%)	N (at%)
$Ni_{0.8}Fe_{0.2}P$-C	2.32	1.38	5.47	73.81	13.94	3.08

Table S2. Metal contents of $Ni_{0.8}Fe_{0.2}P$-C determined by ICP-MS.

Sample	Ni (wt%)	Fe (wt%)	Atomic ratio Fe:Ni
$Ni_{0.8}Fe_{0.2}P$-C	12.29	2.82	7: 29

Table S3. Comparison of electrocatalytic performances of this work with other TMP-based electrocatalysts for HER in alkaline media.

Electrode materials	Current density (j)	Overpotential (η) at (j)	Tafel slope	Stability hours	Electrolyte	Ref.
Ni-Co-P/NF	10 mA cm^{-2}	85 mV	46 mV dec^{-1}	25 h	1.0 M KOH	[1]
FeP/C4-11	10 mA cm^{-2}	95 mV	58 mV dec^{-1}	24 h	1.0 M KOH	[2]
NiFeP	10 mA cm^{-2}	98 mV	99 mV dec^{-1}	30 h	1.0 M KOH	[3]
FeP	10 mA cm^{-2}	116 mV	57 mV dec^{-1}	--	1.0 M KOH	[4]
MnCoP/NiP/NF	10 mA cm^{-2}	119 mV	61 mV dec^{-1}	25 h	1.0 M KOH	[5]
NiFe/CNTs-900	10 mA cm^{-2}	149 mV	87 mV dec^{-1}	12 h	1.0 M KOH	[6]
NiFeP/NFF	10 mA cm^{-2}	155 mV	68 mV dec^{-1}	12 h	1.0 M KOH	[7]
NiFeP@N-CS	10 mA cm^{-2}	186 mV	112 mV dec^{-1}	1000 h	1.0 M KOH	[8]
$Ni_{0.8}Fe_{0.2}P$-C/NF	10 mA cm^{-2}	45 mV	133 mV dec^{-1}	100 h	1.0 M KOH	This work

Table S4. Comparison of electrocatalytic performances of this work with other TMP-based electrocatalysts for OER in alkaline media.

Electrode materials	Current density (j)	Overpotential (η) at (j)	Tafel slope	Stability hours	Electrolyte	Ref.
NiFeP@C	10 mA cm^{-2}	260 mV	39 mV dec^{-1}	20 h	1.0 M KOH	[9]
CoFeP-NC	10 mA cm^{-2}	283 mV	69 mV dec^{-1}	10 h	1.0 M KOH	[10]
2.5Fe-NiCoP/PBA HNCs	10 mA cm^{-2}	290 mV	70 mV dec^{-1}	40 h	1.0 M KOH	[11]
Fe-doped NiO_x nanosheets	10 mA cm^{-2}	310 mV	49 mV dec^{-1}	18 h	1.0 M KOH	[12]
NiFe@CN-G	10 mA cm^{-2}	320 mV	41 mV dec^{-1}	4 h	1.0 M KOH	[13]
Porous Ni_2P	10 mA cm^{-2}	320 mV	105 mV dec^{-1}	10 h	1.0 M KOH	[14]
CoFeP	10 mA cm^{-2}	350 mV	59 mV dec^{-1}	--	1.0 M KOH	[15]
$Fe_{0.5}Ni_{0.5}Co_2O_4$	10 mA cm^{-2}	350 mV	27 mV dec^{-1}	10 h	1.0 M KOH	[16]
$Ni_{0.8}Fe_{0.2}P$-C/NF	10 mA cm^{-2}	242 mV	76 mV dec^{-1}	48 h	1.0 M KOH	This work

Table S5. Comparison of electrocatalytic performances of this work with other TMP-based electrocatalysts for water splitting in alkaline media.

Electrode materials	Current density (j)	Overpotential (η) at (j)	Stability hours	Electrolyte	Ref.
NiFe(1:1)P-MOF	10 mA cm^{-2}	1.54 V	20 h	1.0 M KOH	[17]
MOF CoFeP	10 mA cm^{-2}	1.55 V	30 h	1.0 M KOH	[18]
CoFeP NS@NCNF	10 mA cm^{-2}	1.59 V	15 h	1.0 M KOH	[19]
CoFeP-NC	10 mA cm^{-2}	1.62 V	20 h	1.0 M KOH	[10]
NiP/NF	10 mA cm^{-2}	1.63 V	24 h	1.0 M KOH	[20]
NiFeP@N-CS	10 mA cm^{-2}	1.63 V	24 h	1.0 M KOH	[8]
$NiFeO_x$/NiFeP/NF	10 mA cm^{-2}	1.65 V	15 h	1.0 M KOH	[21]
Ni_5P_4	10 mA cm^{-2}	1.70 V	20 h	1.0 M KOH	[22]
$Ni_{0.8}Fe_{0.2}$P-C/NF	10 mA cm^{-2}	1.56 V	100 h	1.0 M KOH	This work

References

1 C. Yu, F. Xu, L. Luo, H. S. Abbo, S. J. J. Titinchi, P. K. Shen, P. Tsiakaras and S. Yin, *Electrochim. Acta*, 2019, **317**, 191–198.

2 M. H. Suliman, T. N. Baroud, M. N. Siddiqui, M. Qamar and E. P. Giannelis, *Int. J. Hydrogen Energy*, 2021, **46**, 8507–8518.

3 D. W. Wang, Y. Di Zhu, S. Lei, S. M. Chen, Z. G. Gu and J. Zhang, *J. Solid State Chem.*, 2021, **293**, 121779.

4 M. Guo, Y. Qu, C. Yuan and S. Chen, *Int. J. Hydrogen Energy*, 2019, **44**, 24197–24208.

5 Y. Du, W. Wang, H. Zhao, Y. Liu, S. Li, L. Wang and B. Liu, *Chem. - A Eur. J.*, 2021, **27**, 3536–3541.

6 H. Li, Y. He, T. He, H. Shi, H. Yu, X. Ma, Y. Zhang, C. Zhang and S. Wang, *J. Solid State Chem.*, 2020, **289**, 121498.

7 X. Yu, X. He, R. Li and X. Gou, *Dalt. Trans.*, 2021, **50**, 8102–8110.

8 J. Hei, G. Xu, B. Wei, L. Zhang, H. Ding and D. Liu, *Appl. Surf. Sci.*, 2021, **549**, 149297.

9 Q. Kang, M. Li, J. Shi, Q. Lu and F. Gao, *ACS Appl. Mater. Interfaces*, 2020, **12**, 19447–19456.

10 C. Zhao, F. Wei, H. Lv, D. Zhao, N. Wang, L. Li, N. Li and X. Wang, *Materials.*, 2021, **14**, 14061473.

11 D. Li, C. Liu, W. Ma, S. Xu, Y. Lu, W. Wei and J. Zhu, *Electrochim. Acta*, 2021, **367**, 137492.

12 G. Wu, W. Chen, X. Zheng, D. He, Y. Luo, X. Wang, J. Yang, Y. Wu, W. Yan, Z. Zhuang, X. Hong and Y. Li, *Nano Energy*, 2017, **38**, 167–174.

13 A. C. Deng, K. Wu, J. Scott, S. Zhu, R. Amal and D. Wang, *ChemElectroChem*, 2018, **5**, 732–736.

14 Q. Wang, Z. Liu, H. Zhao, H. Huang, H. Jiao and Y. Du, *J. Mater. Chem. A*, 2018, **6**, 18720–18727.

15 Y. Du, H. Qu, Y. Liu, Y. Han, L. Wang and B. Dong, *Appl. Surf. Sci.*, 2019, **465**, 816–823.

16 K. Yan, X. Shang, Z. Li, B. Dong, X. Li, W. Gao, J. Chi, Y. Chai and C. Liu, *Appl. Surf. Sci.*, 2017, **416**, 371–378.

17 X. Xu, T. Wang, C. Zhao, Z. Huang, M. Zheng, R. Jia and Y. Liu, *Microporous Mesoporous Mater.*, 2020, **312**, 110760.

18 A. Muthurasu, G. P. Ojha, M. Lee and H. Y. Kim, *J. Phys. Chem. C*, 2020, **124**, 14465−14476.

19 B. Wei, G. Xu, J. Hei, L. Zhang, T. Huang and Q. Wang, *J. Colloid Interface Sci.*, 2021, **602**, 619–626.

20 J. Ren, Z. Hu, C. Chen, Y. Liu and Z. Yuan, *J. Energy Chem.*, 2017, **26**, 1196–1202.

21 C. Zhang, N. Gong, C. Ding, Y. Li, W. Peng, G. Zhang, F. Zhang and X. Fan, *Int. J. Hydrogen Energy*, 2019, **44**, 26118–26127.

22 M. Ledendecker, S. K. Calderón, C. Papp, H. Steinrück, M. Antonietti and M.

Shalom, *Angew. Chemie*, 2015, **54**, 12361–12365.